Chapter 13
Optical Properties of Intrinsic Excitons in Bulk Semiconductors

Having treated the optical properties of phonons, plasmons and magnons, we come in this and the following chapters to the essence of semiconductor optics, namely the optical properties of excitons.

Phonons are necessary to describe the optical properties of semiconductors and of insulators in the IR; plasmons determine the optical properties of metals from the IR through the visible to the near UV, and in semiconductors, if present at all, they contribute along with the phonons to the IR spectra. Excitons, on the other hand, determine together with their continuum stats or the band-to-band transition the optical properties around and above the band gap, i.e., in the visible including the near UV and IR in the case of semiconductors and in the (V)UV for insulators. Although inorganic insulators like the alkali halides and organic ones such as anthracene have specific optical properties, many of the aspects presented in the following for excitons in semiconductors also apply to them.

We gave at the beginning of Chap. 9 already some information on the history of exciton research. We collect here again some of the early references e.g. [44M1, 52H1, 53U1, 57E1, 57M1, 58D1, 58H1, 59M1, 60H1, 62H1, 62P1, 63H1, 66V1], give some further references for early spectroscopy of semiconductors [40K1, 54K1] and cite some early reviews [63P1, 81R1].

13.1 Excitons with Strong Oscillator Strength

We concentrate in this chapter on the intrinsic linear optical properties of excitons in bulk semiconductors starting from semiconductors with a dipole-allowed, direct band-to-band transition because they exhibit dipole-allowed excitons with the highest oscillator strength. Values of their longitudinal–transverse splitting Δ_{LT} range from 0.1 to beyond 10 meV.

It should be mentioned, however, that not all excitons in this group of semiconductors have high oscillator strength and that some excitons in semiconductors

C.F. Klingshirn, *Semiconductor Optics*, 4th ed., Graduate Texts in Physics,
DOI 10.1007/978-3-642-28362-8_13, © Springer-Verlag Berlin Heidelberg 2012

with dipole-forbidden band-to-band transitions may be dipole allowed, but with considerably lower oscillator strength. We come back to these cases in Sect. 13.2, ending with indirect gap materials.

13.1.1 Exciton–Photon Coupling

In semiconductors with dipole-allowed direct band-to-band transitions, excitons occur, which couple strongly to the radiation field. As a consequence many optical properties can be understood quantitatively only in the strong-coupling or polariton picture. Thus we use this occasion to elucidate once more for this particular case the concept of weak and of strong coupling to the radiation field, heeding the classical dogma "repetitio est mater studiorum".

In Sects. 2.1–2.4 we introduced the electromagnetic radiation field, and in Sect. 2.5 the photons as its quanta. In Chaps. 9–11 we presented the properties of various elementary excitations. The interaction between the two can be treated in perturbation theory. This is the so-called weak coupling approach. The one-photon absorption coefficient $\alpha(\omega)$ is then at resonance proportional to the dipole matrix element squared in (13.1a), i.e., by first order-perturbation theory with the initial and final state:

$$\alpha(\omega) \propto |\langle f \mid H_{\mathrm{D}} \mid i \rangle|^2 \, \delta \left(E_{\mathrm{i}} - E_{\mathrm{f}} + \hbar\omega \right) . \tag{13.1a}$$

The refractive index is obtained at this level of approximation either by a Kramers–Kronig transformation of $\alpha(\omega)$ or, away from the resonance, by second-order perturbation theory according to

$$n^2(\omega) - 1 \propto \sum_{z \neq i} \frac{\langle i \,|\, H_{\mathrm{D}} | z \rangle \, \langle z | H_{\mathrm{D}} | i \,\rangle}{E_z - E_{\mathrm{i}} - \hbar\omega} \tag{13.1b}$$

A photon $\hbar\omega$ creates virtually an excited intermediate state $|z\rangle$ under momentum conservation, which, after a time Δt limited by

$$\Delta E \, \Delta t = |E_2 - E_1 - \hbar\omega| \Delta t \lesssim \hbar \, , \tag{13.2}$$

emits again a photon which is identical to the incident one, while the electronic system returns to the initial state $|i\rangle$. The time Δt during which the energy is "stored" in the virtually excited state reduces the phase velocity of the light and thus evidently describes an $n(\omega)$ which increases when ω approaches the resonance energy $E_z - E_{\mathrm{i}}$ from below, since ΔE goes to zero and Δt can be very long, in agreement with Fig. 4.4.

In the polariton concept, on the other hand, one quantizes the mixed state of the electromagnetic radiation and the excitation of the medium, i.e., the polarization wave. We already introduced this concept in Chap. 5. Since it is a very important one we want to demonstrate it here again for the exciton polariton.

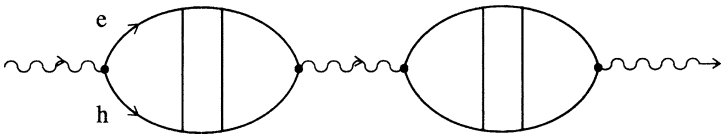

Fig. 13.1 Diagrammatic representation of an exciton polariton

For readers who are not satisfied with the simple statement that the polaritons are the quanta of the mixed states of electromagnetic radiation and excitation (or polarization), we give two other approaches. The first is just a diagrammatic representation of what was said before.

In Fig. 13.1 an incident photon creates an electron–hole pair, which recom-bines again to give a photon, and so on. The Coulomb interaction between electron and hole, which is responsible for the formation of the exciton, is represented by a virtual exchange of photons between electron and hole, i.e., by the vertical lines. Consequently the whole diagram of Fig. 13.1 can be considered as a representation of the exciton polariton.

In the other approach, which follows [93H1] of Chap. 1, we start with the electron and hole operators, construct from them the exciton and finally the exciton polariton (see also Sect. 9.1).

We start with the creation and annihilation operators for excitons:

$$B^{+}_{v,\boldsymbol{k}} \; ; \; B_{v,\boldsymbol{k}} \; . \tag{13.3}$$

The index v stands for the quantum numbers n_{B}, l, m.

It can be shown that the $B_{v,\boldsymbol{k}}$ deviate from the commutator relations of ideal bosons by a term proportional to the mean number of electron–hole pairs, n, contained in the volume of an exciton a^{d}_{B} (see e.g. [93H1, 93P1] of Chap. 1)

$$\langle [B_{0,0}, B^{+}_{0,0}]^{-} \rangle = 1 - \mathrm{O}\,(n a^{d}_{\mathrm{B}})\,, \tag{13.4}$$

where d is the dimensionality of the system. The Hamiltonian of a non-interacting exciton gas is then

$$H = \sum_{v,\boldsymbol{k}} E\,(v, \boldsymbol{k})\; B^{+}_{v,\boldsymbol{k}}\; B_{v,\boldsymbol{k}}\; . \tag{13.5}$$

Using an analogous expression for the photons with the number operator $c^{+}_{\boldsymbol{k}} c_{\boldsymbol{k}}$, for the interacting system of excitons and photons considering the leading, i.e., resonant terms around a specific resonance only, we obtain

$$H = \sum_{\boldsymbol{k}} \left[\sum_{v} E_{v\boldsymbol{k}}\; B^{+}_{v\boldsymbol{k}}\; B_{v\boldsymbol{k}} + \hbar\,\omega_{\boldsymbol{k}}\; c^{+}_{\boldsymbol{k}} c_{\boldsymbol{k}} - \mathrm{i}\,\hbar \sum_{v} g_{v\boldsymbol{k}}\; (B^{+}_{v\boldsymbol{k}}\; c_{\boldsymbol{k}} - h.c.) \right] . \tag{13.6}$$

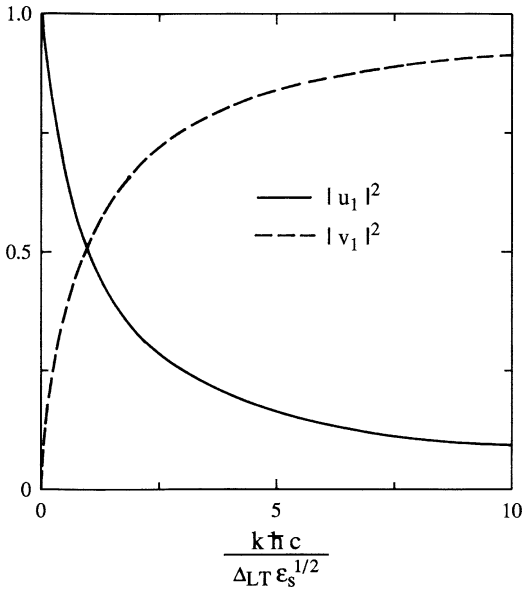

Fig. 13.2 The energy dependence of the $u_{v,k}$ and v_k of (13.7) for the upper polariton branch (According to [93H1] of Chap. 1)

The coupling coefficients g_{vk} contain the transition matrix elements as in (13.1).

If we consider the third term on the right-hand side of (13.6) as a perturbation, we are back once more to the weak coupling limit.

The polariton concept is obtained if we diagonalize the whole Hamiltonian (13.6) by a suitable linear combination of the B_{vk} and the c_k, leading to the polariton operator P_k

$$P_k = u_{vk}\, B_{v,k} - v_k\, c_k \tag{13.7}$$

$$\text{with} \quad |u_{vk}|^2 + |v_k|^2 = 1\,. \tag{13.8}$$

The u_{vk} give the exciton-like character of the polaritons. They are close to one around the exciton energy $E_{v,0}$ and decrease on the upper and lower polariton branches with decreasing energetic distance from the resonance. The v_k give the photon-like part and, according to (13.8), show the opposite behavior. In Fig. 13.2 we give an example for the upper polariton branch. As a rule of thumb we can state that the polariton wavefunction contains considerable exciton-like parts over energies

$$|\,\hbar\,\omega - E_{\text{ex}}\,| \lesssim 10\,\Delta_{\text{LT}}\,. \tag{13.9}$$

It is interesting to note that the dispersion relation that we obtain from this approach is identical to the one obtained from the set of classical coupled oscillators treated in Chaps. 4 and 5.

13.1.2 Consequences of Spatial Dispersion

In contrast to that of optical phonons, the $\boldsymbol{k}$ dependence of the exciton energy is significant. For $\boldsymbol{k}$ vectors in the transition region from the photon-like to the exciton-like part of the dispersion relation, the so-called bottle-neck, the kinetic energy term in (9.1a) becomes comparable to the longitudinal transverse splitting Δ_{LT}. The consequences of spatial dispersion have already been outlined in connection with Figs. 5.3–5.5, so that we can restrict ourselves to just recalling them here. For all frequencies there is at least one propagating mode. This fact reduces the reflectivity in the reststrahlbande to values below 1, even in the case of negligible damping. For frequencies above ω_{L} there are several propagating modes, and below it there is at least one propagating mode and one or more evanescent ones. This situation is not covered by the boundary conditions deduced from Maxwell's equations and additional boundary conditions (abc) have to be introduced containing the information about what fraction of the energy transmitted through the interface travels on which polariton branch. Since this "branching" ratio is ω-dependent and since the imaginary parts of the various branches differ, the decay of the intensity into the depth of the sample can be nonexponential. This means the "effective" absorption coefficient can be thickness dependent. Furthermore it looks more complex (Fig. 5.5) than Fig. 4.4.

The abc which have been introduced by Pekar and by Hopfield [58H1, 62H1, 62P1, 63H1, 64M1] assume that the excitonic part of the polarization at the surface vanishes, or its derivative normal to the surface, or a linear combinations of both. See Sect. 5.4 and e.g. [74A1,75L1,78B1,78H1,78S1,79B1,79S1,80B1,81B1,81L1, 81S1, 82O1, 82R1, 82S1, 83M1, 84H1, 84S1, 85H1] of Chap. 5. In [98H1] a way out of this abc problem has been shown. For even more recent approaches see [00T1, 01S1]. Furthermore one can assume that excitons do not "leak out" of the semiconductor into vacuum and that there should consequently be an exciton-free surface layer (dead layer), the optical properties of which are described by ε_{b} and which has a minimum thickness of the excitonic Bohr radius. Electric fields, which occur often at surfaces normal to them, can ionize, i.e., destroy the exciton and lead to an increase in the thickness of the dead layer. The problem which thus has to be solved to calculate a reflection spectrum is shown in Fig. 13.3. An incident beam passes first the dead layer in which multiple reflection occurs and then enters the semiconductor in which several modes can be excited. Sometimes scientists apply even more complex models assuming, e.g., that the damping and/or the eigenfrequencies are depth dependent [79E1, 81L1, 82S1].

The formulas to calculate the spectra are rather complex and we do not give them here but refer the reader to [75L1,78S1,79E1,80B1,81L1,82B1,82S1,84R1,85H1, 93K1, 95B1] or the references from Chap. 5 given above. Instead we give in the next section examples of reflection, transmission, and luminescence spectra of the exciton polariton in bulk semiconductors with direct, dipole-allowed band-to-band transitions.

In [04S1] it has been suggested that the exciton free layer may be absent at interfaces between similar materials.

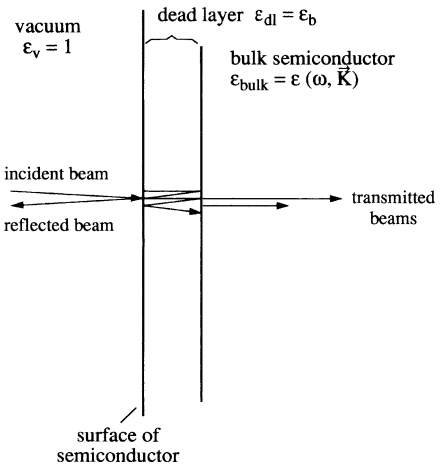

Fig. 13.3 The problem of reflection for a semiconductor in the vicinity of an exciton resonance for normal incidence including multiple reflection in a dead layer and two propagating modes due to spatial dispersion

13.1.3 Spectra of Reflection, Transmission and Luminescence

In Fig. 13.4a we show the bandstructure of CdS and in part b the dispersion of the exciton polariton for the orientation $\boldsymbol{k} \perp \boldsymbol{c}, \boldsymbol{E} \perp \boldsymbol{c}$ and including the $n_B = 1$ excitons involving a hole either in the A or in the B valence band. The A exciton is a rather simple resonance for this orientation, comparable to our model system in Sect. 5.2. The k-linear term of the B valence band (Sect. 8.8) mixes the singlet and triplet states for $\boldsymbol{k}_\perp \neq 0$ (see Sect. 13.2.1.1) and gives rise to an additional polariton branch. Figure 13.4c finally gives the reflection spectra of the two resonances for $\boldsymbol{E} \perp \boldsymbol{c}$ and $\boldsymbol{E} \parallel \boldsymbol{c}$ and of some higher states ($n_B \geq 2$). The combination of the Γ_1 (S-) envelope function for $n_B = 1$ with the symmetries of the electron Γ_7 and the holes (AΓ_9, BΓ_7) gives excitons of symmetries AΓ_5 and AΓ_6 and BΓ_1, BΓ_2, BΓ_5 as explained in more detail in Chap. 26. The Γ_6 and Γ_2 states are triplets which couple only weakly to the radiation field since they are spin-flip and dipole-forbidden and do not show up in reflection (see Sect. 13.2.1.1). Γ_5 and Γ_1, states couple to the radiation field for the orientations $\boldsymbol{E} \perp \boldsymbol{c}$ and $\boldsymbol{E} \parallel \boldsymbol{c}$, respectively. These selection rules show up clearly in the reflection spectra, the $n_B = 1$ A excitons being seen only in $\boldsymbol{E} \perp \boldsymbol{c}$.

A fit to the reflection spectra (not shown here) using spatial dispersion, an exciton-free layer and some abc coincides with experiments within a few percent.

The AΓ_5 resonance is quite simple, as already mentioned. R remains significantly below 1 due to spatial dispersion as predicted above. For smaller oscillator strength or longitudinal-transverse splitting, the maximum almost disappears and only a narrow dip close to the longitudinal eigenfrequency remains, as shown in Fig. 13.5 for ZnTe.

The small spike around AΓ_5^L in Fig. 13.4c is partly caused by the onset of the UPB but mainly by the dead layer. An increase of its thickness increases the

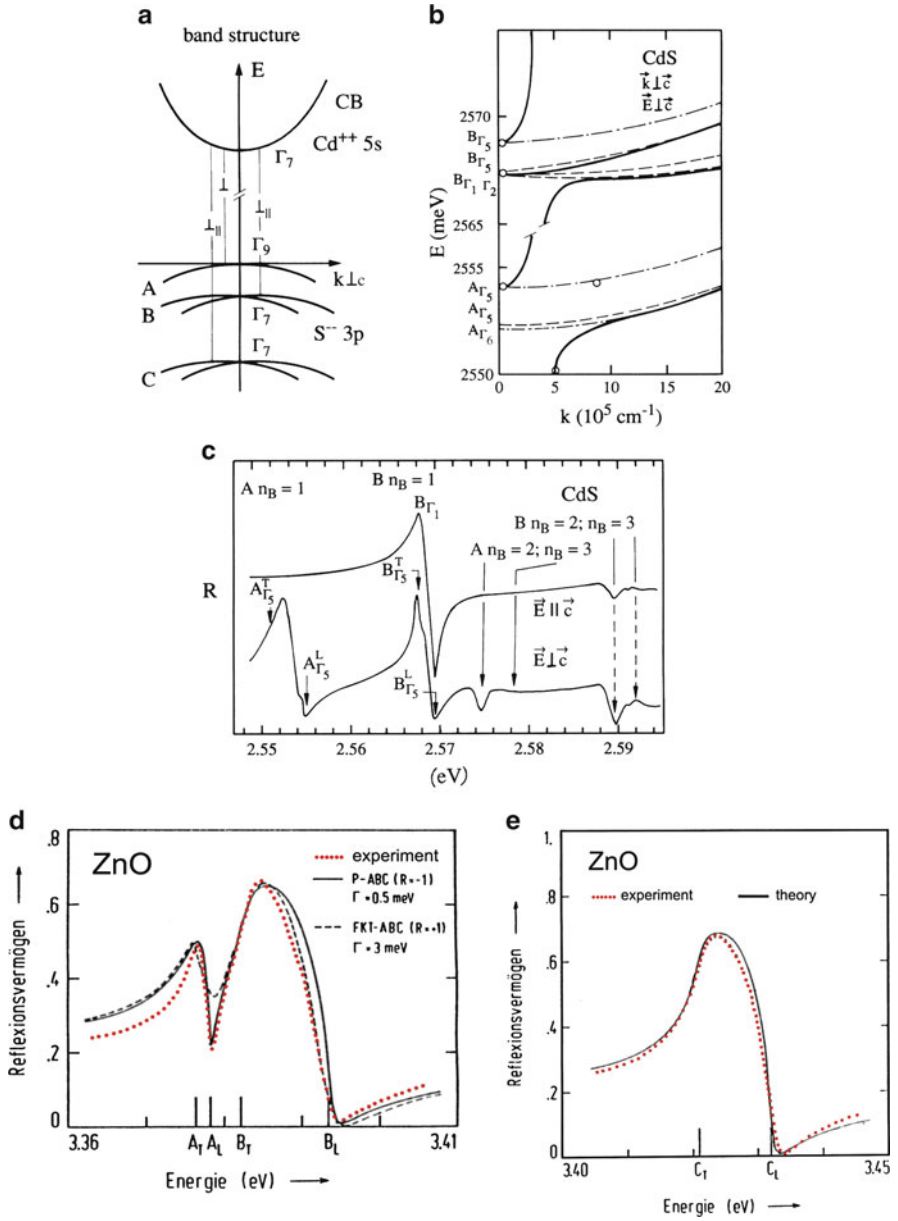

Fig. 13.4 The bandstructure of CdS around the Γ-point (**a**); the dispersion of the $n_B = 1$ A and B exciton polariton resonances (**b**); the reflection spectra for the polarizations $\boldsymbol{E} \perp \boldsymbol{c}$ and $\boldsymbol{E} \parallel \boldsymbol{c}$ (**c**) and the reflection spectra for ZnO for the $n_B = 1$ exciton resonances in both orthogonal polarizations (**d**, **e**). According to [82B1,85H1,93K1] (**a–c**) and to [73H1,75L1,78H1,78H2,82B1] (**d**, **e**)

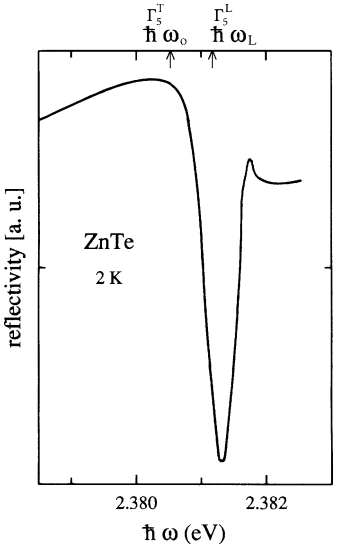

Fig. 13.5 A reflection spectrum for ZnTe. According to [83M1]. For the dispersion of the exciton polariton see Sect. 16.1.1

importance of the spike due to multiple reflections (Fig. 13.3) and may even lead to an "inversion" of the usual reflection spectrum, i.e., to a dip at low energies and a maximum above. A set of calculated spectra showing this phenomenon is given in Fig. 13.6.

The BΓ_1 exciton resonance is again a simple one, but the BΓ_5 has a small dip stemming from the additional polariton branch shown in Fig. 13.4b, which at this energy reaches exactly $n = 1$.

While the A and BΓ_5 excitons have in CdS for $\boldsymbol{E} \perp \boldsymbol{c}$ roughly equal oscillator strength and Δ_{LT} [85H1], the situation changes for close lying resonances as occurs for ZnO [85H1]. In this case the longitudinal transverse splitting Δ_{LT} of the AΓ_5 exciton is reduced and that of the BΓ_5 increased as discussed already in Sect. 4.5. Only the sum of $\Delta_{\mathrm{LTA}\Gamma_5}$ and $\Delta_{\mathrm{LTB}\Gamma_5}$ has to be constant and equal to $\Delta_{\mathrm{LTC}\Gamma_1}$ [60H1]. To illustrate this statement, Fig. 13.4d and e shows a close-up of the $n_{\mathrm{B}} = 1$ exciton reflection spectra for the two orthogonal polarizations $\boldsymbol{E}$ perpendicular and parallel to $\boldsymbol{c}$. Note the different selection rules foe CdS and ZnO, resulting from a pecularity of the valence band ordering in ZnO. After a long debate over several decades on the normal or inverted valence band ordering in ZnO, the inverted ordering is now generally accepted. We do not go in this general textbook on semiconductor optics into details of this peculiarity, but refer the reader to Chaps. 4 and 6 of [10K2], to [81R1, 10K1] and the references given therein.

At higher energies we see $n_{\mathrm{B}} \geq 2$ exciton states which split into several sublevels due to the various L and/or L_z values of the envelope function. The reflection signal of these higher states decreases due to the n_{B}^{-3} dependence of the oscillator strength [57E1]. In the band-to-band transition region the reflection spectra are usually flat and structureless. The C-excitons expected for CdS from Fig. 13.4a are situated around 2.61 eV and are off the scale of Fig. 13.4b and c. These resonances

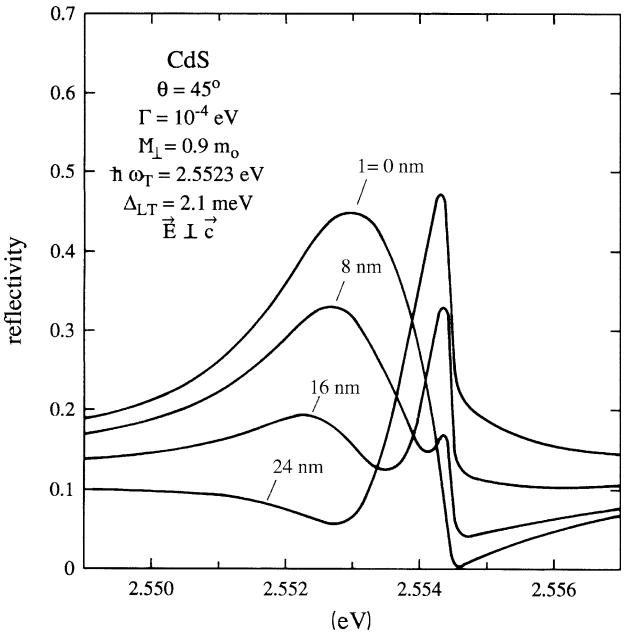

Fig. 13.6 A set of calculated exciton reflection spectra of CdS for 45° incidence and for various thicknesses of the exciton-free layer with all other parameters kept constant (According to [82R1])

are washed out even at low temperature because the C-exciton is situated in the continuum of the A- and B-excitons and thus has a rather short phase relaxation time T_2, i.e., strong damping. For the case of ZnO the $C\Gamma_A$ exciton is shown in Fig. 13.4e.

With increasing lattice temperature the exciton resonances are broadened due to increasing scattering with phonons. Sometimes they are hardly visible at RT as shown in Fig. 13.7 for CdS similar data are also found for ZnO e.g. in [80B2]. A similar washing out of the exciton resonance can occur even at low temperatures in samples with high impurity content and/or lower crystalline quality or for increasing excitation desenty.

We come back to the temperature dependence of the damping of excitons [90R1] in connection with luminescence below. For the temperature dependence of the band gap itself see e.g. [67V1, 99P1, 07K1, 10K1, 10K2] and references therein.

Many more examples of excitonic reflection spectra for III–V-, II–VI- and I–VII compounds are found e.g. in the references above, in [77V1, 79V1, 80B1, 80D1], in Figs. 13.5–13.7, in [74B1] for AgI, in the reviews [81K1, 85H1] cited in Chap. 9, or in the data collection [82L1] and textbook [86U1] of Chap. 1.

To summarize, we can state that the reflection spectra of semiconductors are determined around the gap by exciton polaritons. The longitudinal eigenenergy can be reasonably well determined from the reflection minimum which corresponds to $n = 1$ on the UPB and is therefore situated only slightly (<1 meV) above $\hbar\omega_L$. The

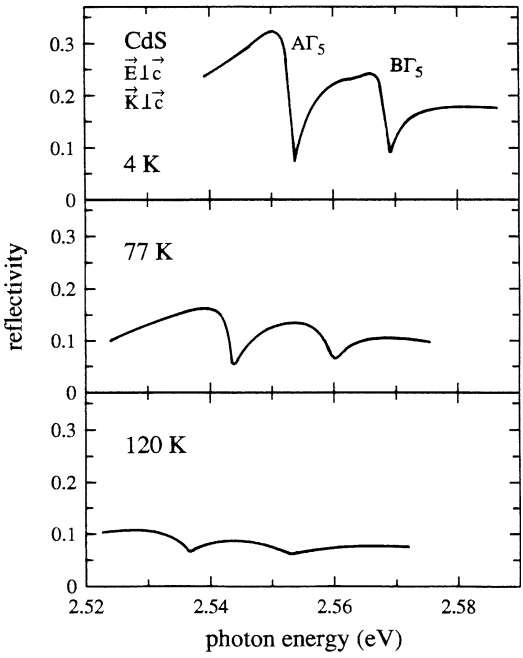

Fig. 13.7 A set of reflection spectra of the A- and B-exciton resonances of CdS for various lattice temperatures (According to [80B2])

transverse eigenenergy, the oscillator strength, the damping, and the effective mass of the exciton can be extracted only with the help of a rather complicated line-shape analysis.

For uniaxial, hexagonal materials like CdS or ZnO it can be shown from group-theoretical considerations that the Γ_5-excitons are the resonances for the ordinary beam (Sect. 3.1.7) because the polarization $\boldsymbol{E} \perp \boldsymbol{c}$ can be realized for all angles between $\boldsymbol{k}$ and $\boldsymbol{c}$. The Γ_1 resonances have dipoles oriented parallel to $\boldsymbol{c}$. As a consequence they have maximum coupling to the radiation field for $\boldsymbol{E} \parallel \boldsymbol{c}$ and $\boldsymbol{k} \perp \boldsymbol{c}$, but develop as extraordinary or mixed-mode polaritons to the longitudinal state if the angle $\angle(\boldsymbol{k}, \boldsymbol{c})$ is continuously changed from $\boldsymbol{k} \perp \boldsymbol{c}$ to $\boldsymbol{k} \parallel \boldsymbol{c}$. In Fig. 13.8 we show the dispersion of the CΓ_1 exciton polariton in ZnO, which has an oscillator strength varying according to

$$\Delta_{\mathrm{LT}} = \Delta_{\mathrm{LT}}^{0} \sin^2 \angle(\boldsymbol{k}, \boldsymbol{c}) \,. \tag{13.10}$$

The complimentary angle dependence holds for the A and B Γ_5 excitons for the orientation of $\boldsymbol{E}$ in the main section i.e. for extraordinary beams.

Experimental data for mixed mode polaritons can be found in [72W1, 75L1]. The small refection spike seen at B$\Gamma_{5\mathrm{L}}$ in [03C1] might similarly well be due to a mixed mode polariton due to the finite angle of aperture of the incident beam. See for a more exhaustive discussion of the reflection spectra of ZnO the references [07K1, 10K1, 10K2] cited already above.

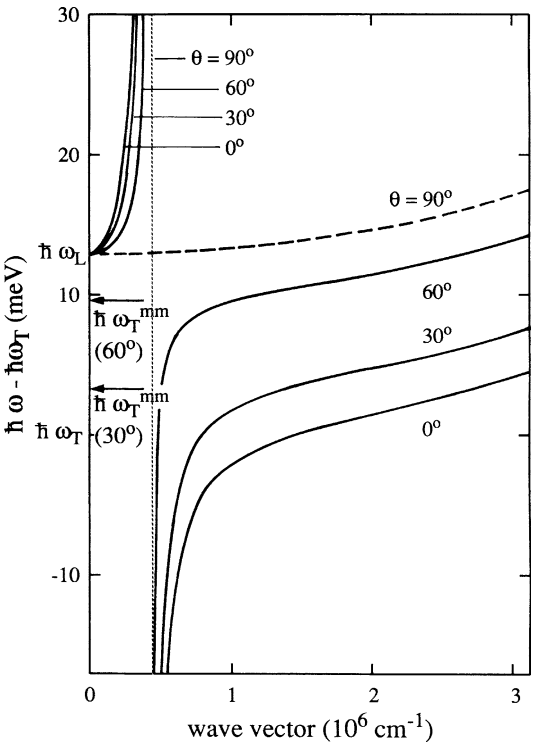

Fig. 13.8 Dispersion of the exciton polariton in a uniaxial material for various angles between $\boldsymbol{k}$ and $\boldsymbol{c}$. Data for the CΓ_1 exciton polariton in ZnO (According to [78H1])

The absorption spectra of $n_B = 1$ polariton resonances are usually difficult to measure quantitatively, since in the resonance region the effective absorption, or rather extinction, coefficient reaches values in the range

$$10^4\,\mathrm{cm}^{-1} \lesssim \alpha_{\mathrm{eff}} \lesssim 10^6\,\mathrm{cm}^{-1}\,. \tag{13.11}$$

As a consequence for samples with $d \gtrsim 1\,\mu\mathrm{m}$, the transmitted light intensity goes to "zero", i.e., to values comparable to or smaller than the stray light of the spectrometer. We show in Fig. 13.9a an absorption spectrum of a ZnO layer at RT. The layer is of polycrystalline nature, produced by evaporating Zn on a substrate of quartz glass and subsequent oxidation [44M1]. The crystallites have their $\boldsymbol{c}$ axis oriented perpendicular to the substrate. The peak at 3.3 eV is due to the close lying and thermally broadened AΓ_5 and BΓ_5 exciton resonances [68L1, 75L1, 78H1, 80B1, 81L1, 82B1, 85H1, 03C1] and references therein). This is possibly one of the first experimental observations of a Wannier exciton in absorption, though the author of [44M1] was most probably not aware of this fact. See also Sect. 9.1. In Fig. 13.9b experimental transmission spectra are shown A and BΓ_5 resonances of a thin CdS platelet type sample. There are Fabry–Perot modes (see Sect. 3.1.6) in the transparent region due to the natural reflectivity of the surfaces of the as-grown platelet type sample. A detailed analysis of $\alpha_{\mathrm{eff}}(\omega)$ in the

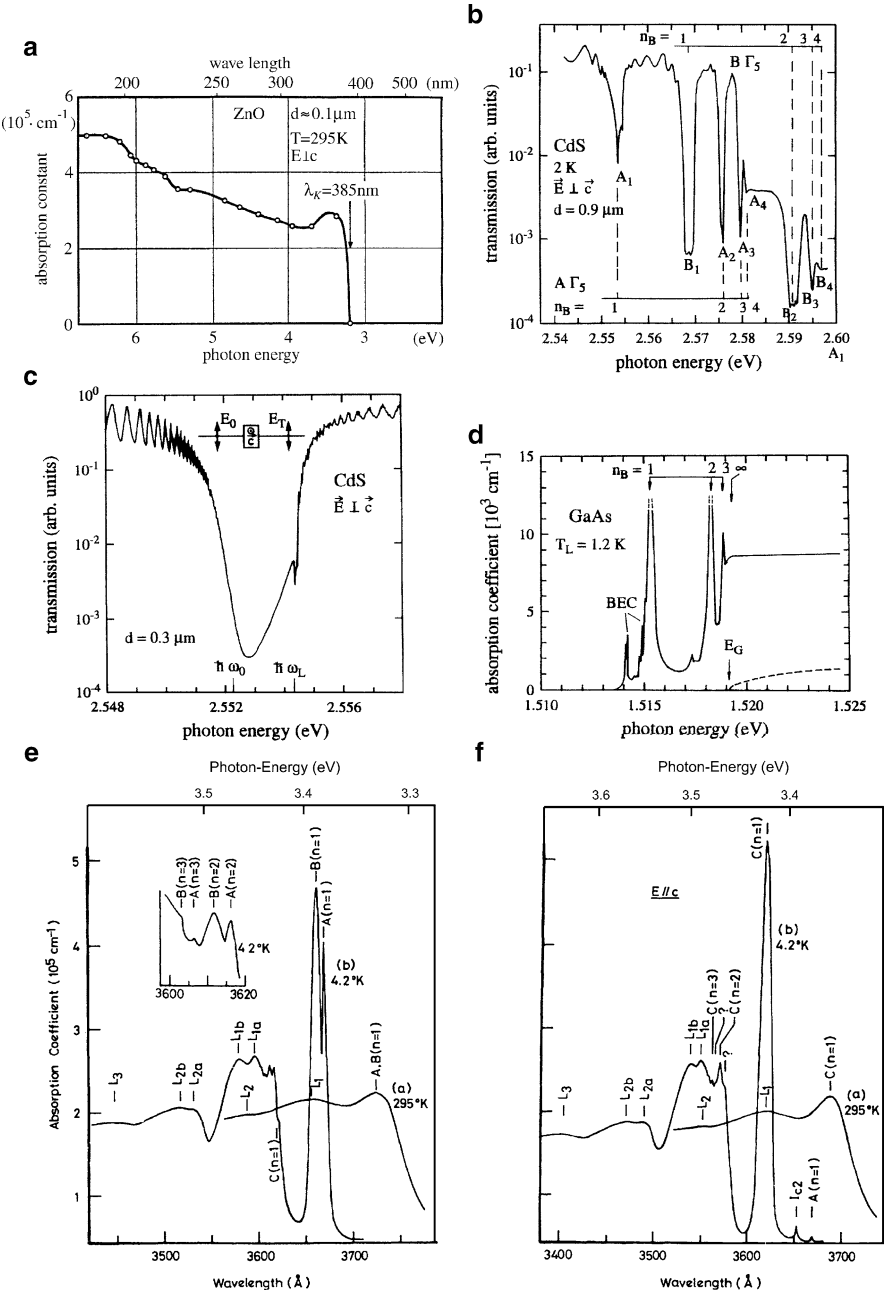

Fig. 13.9 An early experimental absorbtion spectrum of ZnO at RT (**a**), an experimental transmission spectrum of CdS for the orientation $\boldsymbol{E} \perp \boldsymbol{c}$ in the region of the A and B exciton resonances (**b**); a calculated one for the AΓ_5 resonance for $n_B = 1$ (**c**); an absorption spectrum for a thin GaAs sample (**d**) and absorption spectra of ZnO for both polarizations and for 4.2 K and 295 K (**e**,**f**) (According to [44M1], to [79V1, 82R1], [91U1] and to [68L1], respectively)

resonance region is possible only for sample thicknesses of the order of 1 μm, such that $\alpha d \lesssim 4$. Such samples cannot usually be produced by grinding and polishing of thicker samples, since these processes introduce so much damage to the lattice that the damping γ of the resonance becomes too large (i.e., $\hbar\gamma > \Delta_{LT}$).

Sometimes epitaxial layers can be used for this type of investigation, but care has to be taken that these layers do not contain (inhomogeneous) strain since transmission measurements integrate over the whole sample thickness. Fortunately some semiconductors, such as ZnO, CdS or CdSe, tend to grow as thin, single crystal platelets. The absorption spectrum of Fig. 13.9b stems from such a sample. Figure 13.9c shows a calculated tranmission spectrum of the $A\Gamma_5$ $n_B = 1$ resonance. The similarity to the A_1 resonance in Fig. 13.9b and the deviations from the simple case without spatial dispersion of Figs. 4.4 or 11.1 are evident. In Fig. 13.9d we give an overview of the absorption spectrum of a thin GaAs sample. GaAs has, in comparison to CdS or ZnO, a much lower oscillator strength due to the larger value of a_B (see Sect. 9.1); (Δ_{LT} GaAs $\approx$ 0.1 meV). Therefore it is easier to measure the absorption of the $n_B = 1$ exciton. We can see in this figure similarly as for CdS in Fig. 13.9b also the $n_B = 2$ and 3 levels with S-envelope function. Even higher states ($n_B > 3$) merge with the continuum. The decrease of the oscillator strength with n_B^{-3} [57E1] is at least qualitatively confirmed by this spectrum.

In Fig. 13.9e and f we show finally absorption spectra of a thin ZnO platelet for the two main polarizations and for 4.2 and 295 K. One sees again the Rydberg series at 4.2 K up to $n_B = 3$ followed by higher energy structures involving LO phonons. If the coupling to Lo phonons is strong enough, exciton-phonon bound states may develop [68T1, 72K1, 82J1]. Similar structures have been observed in the Cu-halides [66R1, 72B1] or in the photoluminescence excitation spectra of CdTe and CdS [75H1] or in PbI_2 [94W1] and references therein. See also Fig. 15.4.

At higher temperatures the finer details of the absorption spectra are washed out due to the increasing homogeneous broadening resulting from the scattering with thermally excited phonons. One is then left essentially with the broadened $n_B = 1$ exciton states followed by their ionization continuum. Compare Fig. 13.9a with Fig. 13.9e for 295 K.

The rather constant value of α (ω) in the region of the continuum states comes from the product of the square root combined density of states (the dashed line in Fig. 13.9d gives the calculated absorption spectrum for a simple band-to-band transition without Coulomb effects for comparison) and the Sommerfeld factor, already discussed in Sect. 9.3 for $d = 3$.

At higher temperatures, the excitons develop an absorption tail to lower photon energies, which is described by the so-called Urbach or Urbach–Martienssen rule [53U1, 57M1, 58D1, 71K1, 71S1, 72D1, 73J1, 85L1]

$$\alpha(\hbar\omega) = \alpha_0 \exp\left[-\sigma\,(T)\,(E_0 - \hbar\omega)/\,k_B\,T\right], \qquad \hbar\omega < E_0 \tag{13.12}$$

where α_0 and E_0 are material parameters. E_0 is an energy situated several 10 meV above the energy of the lowest free exciton at $T_L = 0$ K. σ is a function varying

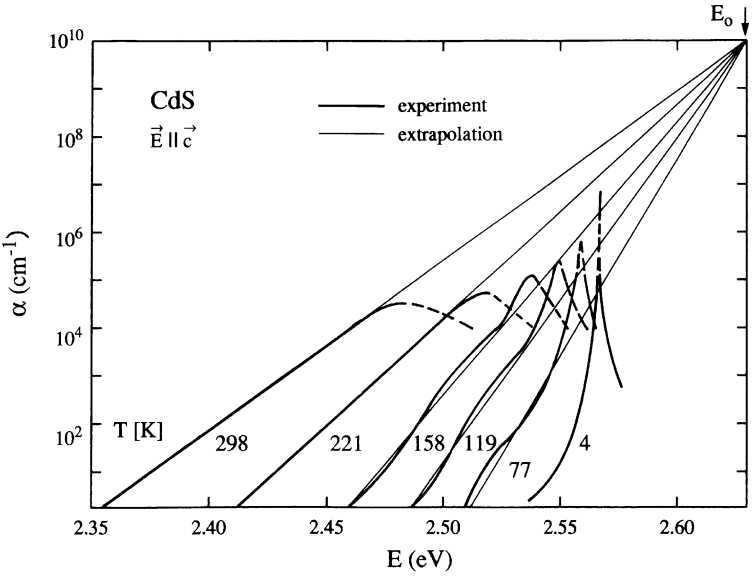

Fig. 13.10 The absorption edge of CdS for various temperatures and the polarization $\boldsymbol{E} \parallel \boldsymbol{c}$ (According to [76S1])

only weakly with temperature. An example is given in Fig. 13.10 for CdS or for ZnO in [73J1].

The temperature dependence of the band gap, which can also be nicely seen in Figs. 13.7, 13.9 or 13.10, is already incorporated in (13.12) since the exciton peak shifts in parallel to the gap.

The reason for the behavior described by (13.12), which is of rather universal nature in semiconductors and insulators, is the interaction of excitons with optical phonons. Two effects are usually discussed in theory: a momentary localization of the excitons in the randomly fluctuating field of optical phonons, or an ionization in their electric field. These two effects seem to contribute with a weight that depends on the material parameters. Details about the theory can be found in [71S1, 72D1, 85L1] and references therein.

There is presently a certain misconception in parts of the literature concerning the interpretation of the low energy absorption tail in semiconductors, especially in the work on ZnO and its alloys. This point has been addressed in detail in Chap. 6 of [10K2] and in [07K1, 10K1]. We summarize the main point here. We understood already, that a simple square root absorption edge starting at the band gap is never observed in semiconductors due to the electron-hole Coulomb interaction, which results in exciton states below the gap and modifies the band-to-band transitions above the gap i.e. in the excitonic ionization continuum. See Sect. 9.3. Furthermore, we understood that an absorption tail develops below the exciton resonance due to interaction with phonons (the Urbach tail, see (13.12) above) and later in Sect. 14.4

we shall see, that disorder contributes additionally to this tail. Several authors tend now to fit this essentially exponential tail with either a simple square root absorption edge or a formula valid for the Tauc regime (see Sect. 14.4 or the references above), extrapolate this fit to absorption coefficient zero and claim that this value gives the band gap or an "optical gap". It is clear from our knowledge of the near edge absorption spectrum of semiconductors, that this approach is fundamentally wrong. So it is not surprising, that this fit coincides with the experimental data indeed usually only over a very limited range of absorption coefficients (frequently less than a factor of 3) and that the thus obtained values of the band gap are systematically too small compared to the true value. The true values are frequently rather precisely known (e.g. for many III–V or II–VI compounds, see reference [82L1] of Chap. 1). Furthermore the absorption coefficient measured at the thus obtained "band gap" is orders of magnitude smaller compared to the correct value which is for ZnO e.g. around 2 $10^5\,\mathrm{cm}^{-1}$ as seen from Fig. 13.13a, e, and f. We shall come back to these aspects shortly in Sect. 14.4.

The absorption of direct excitons in indirect materials will be addressed in Sect. 13.2.2.

The investigation of the luminescence from excitons or more precisely exciton polaritons is a rather difficult task. For early investigations see [72B2, 72W2]. The emission from these states is generally very weak even at low temperatures even in high quality sampels. This has various reasons: the total luminescence yield η_{lum} of semiconductors is often very low. Frequently one finds, even for direct gap materials,

$$10^{-1} \gtrsim \eta_{\mathrm{lum}} \gtrsim 10^{-3}\,, \tag{13.13}$$

i.e., the main recombination channel is non-radiative involving defect centers. A large part of the emission stems from phonon replica and, especially at low temperatures, from bound-exciton complexes, donor–acceptor pairs, or other defect centers which are considered in Chap. 14. Furthermore, the direct emission from free exciton polaritons is limited by various effects: One is the internal reflection, another the small escape depth. These points will be further clarified below.

If we excite an electron–hole pair, e.g., in the continuum states, it will relax to lower energies and thermalize by emission of phonons, as described in more detail in Chap. 23. At very low temperatures ($k_{\mathrm{B}}T < \Delta_{\mathrm{LT}}$) the excitons end up on the LPB where they further relax by acoustic phonon emission. Since the scattering matrix element and the density of final states both decrease in the transition region between exciton- and photon-like dispersion, the excitons accumulate there. This is the reason why this region is called a bottle-neck. At higher temperatures the excitons reach essentially a Boltzmann-like distribution on the exciton-like part of the LPB, on the longitudinal branch, and on the UPB. In the polariton picture the luminescence from these states cannot be described as a "recombination" of the exciton polariton with emission of a photon, since the photon will be immediately reabsorbed to form an exciton, or in other words, since we are considering the quanta of the mixed state of exciton and photon. Strictly speaking, an exciton polariton cannot simply recombine radiatively.

The proper description is the following: The exciton polariton moves with its group velocity through the sample. It can be scattered by impurities or phonons or be trapped. Eventually it reaches the surface. In most cases it will be reflected back into the sample. The limiting angle for total internal reflections α_{TR} is, e.g., for $n = 5 - a$ typical value on the LPB in the bottle neck region as shown in Sect. 13.1.4, only about 13°. Of the excitons impinging under an angle smaller than α_{TR} a considerable fraction are also reflected back into the sample, as becomes clear if one considers the formulas for the reflection under normal incidence or if one integrates over Fresnel formula of Sect. 3.1.4.

Furthermore, the luminescence yield of free-exciton polaritons is limited by the small escape depth l_{esc}, i.e., the depth from which they can reach the surface. If one excites in the band-to-band transition region, the exciting light penetrates about 0.1–1 μm into the sample corresponding to α-values of 10^4–10^5 cm^{-1} in this spectral range. By diffusion, the excitons spread out over a region of 1–2 μm. The depth from which they can reach the surface is much less than this. A rough estimate can be obtained either from the inverse effective absorption coefficient in the exciton resonance or from the product of phase-relaxation time T_2 (Sect. 23.1) and the group velocity in the exciton resonance (Sect. 13.4):

$$\alpha_{\text{eff}}^{-1} = (10^4 - 10^6\,\text{cm}^{-1})^{-1} = 0.01 - 1\,\mu\text{m} \tag{13.14a}$$

$$l_{\text{esc}} = v_g T_2 = (10^{-3} - 10^{-5} \cdot c)\,(10 - 40\,\text{ps}) = (10 - 0.03)\,\mu\text{m} \tag{13.14b}$$

In spite of all these difficulties it was possible to observe the emission from the exciton polariton in many semiconductors and even its temperature dependence [84M3]. We give an example for ZnO in Fig. 13.11. On the left the dispersion relation of the A-exciton is shown for $\boldsymbol{k} \perp \boldsymbol{c}$ and $\boldsymbol{k} \parallel \boldsymbol{c}$ and for the polarizations $\boldsymbol{E} \perp \boldsymbol{c}$ and $\boldsymbol{E} \parallel \boldsymbol{c}$. Since the Γ_7 and Γ_9 valence bands are inverted in ZnO as compared to other Wurtzite type II–VI and III–V semiconductors like CdS, CdSe or GaN, see Sect. 8.8 or Fig. 13.4b, the k-linear term appears in the A-exciton for the orientation $\boldsymbol{k} \perp \boldsymbol{c}$. The influences of the resulting additional polariton branch, of the longitudinal branch, and of the UPB are seen by comparison with the orientation $\boldsymbol{k} \parallel \boldsymbol{c}$ where the longitudinal branch and the k-linear term are missing. A luminescence polarized $\boldsymbol{E} \parallel \boldsymbol{c}$ in the A exciton resonance observed in Fig. 13.11e, f is attributed to the $A\Gamma_1$ exciton, which is dipole allowed for $\boldsymbol{E} \parallel \boldsymbol{c}$ but has in ZnO a much smaller oscillator strength because it involves in this material a spin flip. Consequently both the spectral width and the longitudinal transverse splitting are much narrow. See also [10K1,10K2] and references therein. A similar luminescence has been observed also in [03C1, 04K4]. Some other examples for the polariton luminescence including also other materials, both as bulk samples and epitaxial layers are found e.g. in [68V1, 74S1, 74T1, 75K1, 76S3, 77V1, 79P1, 80D1, 83M2, 95S1, 95S1, 97N1, 97N1, 97N2, 98M1, 99R1, 00T1, 01R1, 01S1, 04K4, 07K1, 10K1, 10K2]. The influence of a k-linear term has been discussed where applicable e.g. in [76S3, 82K1] or in the references given with Fig. 13.11.

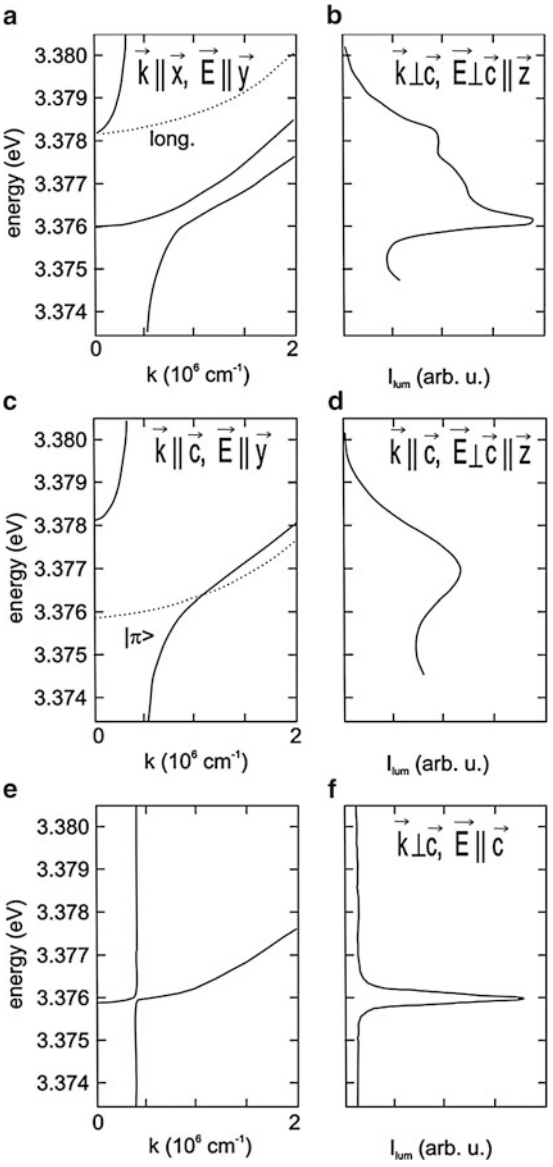

Fig. 13.11 The dispersion of the $n_B = 1$ A-exciton resonance in ZnO for various polorizations $\boldsymbol{E} \perp \boldsymbol{c}$ (**a**–**d**) and orientations $\boldsymbol{k} \perp \boldsymbol{c}$ (**a**,**b**) or $\boldsymbol{k} \parallel \boldsymbol{c}$ (**c**,**d**) and for $\boldsymbol{E} \parallel \boldsymbol{c}$ (**e**,**f**) (According to [78H1, 81K1, 10K1, 10K2])

A luminescence channel of the exciton polaritons with higher luminescence yield at low temperatures in semiconductors with strong exciton-LO phonon coupling are the LO-phonon replicas [68S1]. In this case a polariton on the exciton-like part of the dispersion relation or in the bottleneck is scattered onto the photon-like branch by emission of one or more longitudinal optical phonons. The coupling with this type of phonon is stronger than with transverse optical or acoustic phonons since the lattice

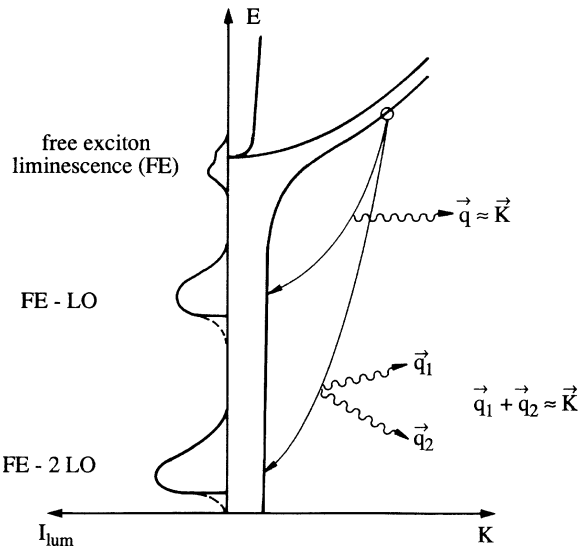

Fig. 13.12 Schematic drawing of the decay mechanisms of the exciton-mLO phonon emission processes

distortion of the polaron (Sect. 8.6) can be described largely as a superposition of longitudinal optical phonons. Once the polariton is on the photon-like branch, it travels over long distances with almost negligible damping and is transmitted through the surface into vacuum with quite high probability, since $n \lesssim 2$ in the corresponding spectral range.

In Fig. 13.12 we show the appearance of the LO-phonon satellites schematically. If we neglect the bottleneck region and homogenous broadening for the moment, we can deduce with the Boltzmann occupation probability the distribution of the excitons as a function of their kinetic energy $E_{\rm kin}$

$$N(E_{\rm kin}) \propto \begin{cases} E_{\rm kin}^{1/2} \exp\{-E_{\rm kin}/k_{\rm B}T\} & \text{for } E_{\rm kin} \geq 0 \\ 0 & \text{otherwise} \end{cases}$$

$$\text{with } E_{\rm kin} = \frac{\hbar^2 \boldsymbol{k}^2}{2M} . \tag{13.15a}$$

The lineshape of the luminescence of the m-th LO-phonon replica is then given by [82P1, 06H1, 07K1]:

$$I_m^{\rm lum}(\hbar\omega) \propto \begin{cases} E_{\rm kin}^{1/2} \exp(-E_{\rm kin}/k_{\rm B}T) W_m(E_{\rm kin}) & \text{for } E_{\rm kin} \geq 0 \\ 0 & \text{otherwise} \end{cases}$$

$$\text{with } \hbar\omega = E_0 - m\hbar\omega_{\rm LO} + E_{\rm kin} . \tag{13.15b}$$

where E_0 is the energy of the dipole allowed, transverse exciton at $\boldsymbol{k} = 0$.

For the explicite discussion of uniaxial crystals see [97G1].

The transition probability $W_m(E_{\rm kin})$ can be often expressed by a power law [82P1], i.e.,

$$W_m(E_{\rm kin}) \propto E_{\rm kin}^{l_m} . \tag{13.16}$$

For $m = 1$ one finds $l_1 = 1$ since the density of final states for the LO phonons increases with $E_{\rm kin} \propto k^2$ assuming that the wave vector of the photon-like exciton polariton in the final state is negligible.

For $m = 2$ many different combinations of the two-phonon wave vectors are possible for a given $\boldsymbol{k}$ of the exciton-like polariton. As a consequence l_2 is zero and the lineshape of the second LO phonon replica directly reflects the distribution of exciton polaritons in the initial state. Finally $I_m^{\rm lum}$ has to be convoluted with a Lorentian, describing the temperature dependent homogenous damping $\Gamma(T)$ as shown e.g. in [06H1, 07K1, 07K2, 10K1, 10K2]. In Fig. 13.13 we show the emission of ZnO for various temperatures. At 110 K (Fig. 13.13a) the bound exciton emission around 3.35 eV is almost gone (compare to Fig. 14.2) and the near edge luminescence is dominated by the homogeneously broadened zero phonon lines of the emission, which are still spectrally resolved, and by their LO phonon replica. The fit coincides nicely with experiment. This coincidence confirms very well the concepts developed above and especially that the excitons are good quasi-particles at low densities (for higher densities see Chaps. 19–21), the distribution of which on their dispersion relation can be described in many cases by Boltzmann statistics in close analogy to an ideal gas. A further example will be given for Cu_2O in Sect. 13.2. The value of the homogeneous broadening deduced from the Lorentzian fit of the zero phonon emission has been used in Fig. 13.13a–c in the convolution of the LO phonon replica (13.15). The energy of the LO phonon (72 meV) is seen in the energetic distance from the zero phonon line to the low energy sides of the X-mLO replica, typically the points of inflection.

With further increasing temperature, homogeneous broadening increases (see Fig. 13.13b, c) and a discrepancy between experiment and theory develops on the high energy side which is due to the reabsorption by the temperature dependent Urbach tail (see above).

At room temperature (RT) the zero phonon emission and its replica merge to an almost unstructured band with a maximum at (3.29 ± 0.02) eV and a FWHM of (90 ± 10) meV. Larger half widths reported by some authors at RT are indicative for additional inhomogeneous broadening presumably due to poor sample quality.

Note that the maximum of the emission at RT is not identical with the free exciton energy at this temperature.

The homogeneous broadening (HWHM) is plotted in Fig. 13.13d as a function of temperature and with the fit function [90R1] and parameters given in this figure. The value of the homogeneous broadening (which must not be confused with the longitudinal transverse splitting) of the A and B Γ_5 exciton polaritons starts at 0 K with a value Γ_0 around 1 meV for high quality bulk samples and epilayers but increases rapidly with temperature and reaches at RT a value of more than 20 meV HWHM! See for a detailed discussion of the parameters e.g. [07K1, 10K1, 10K2].

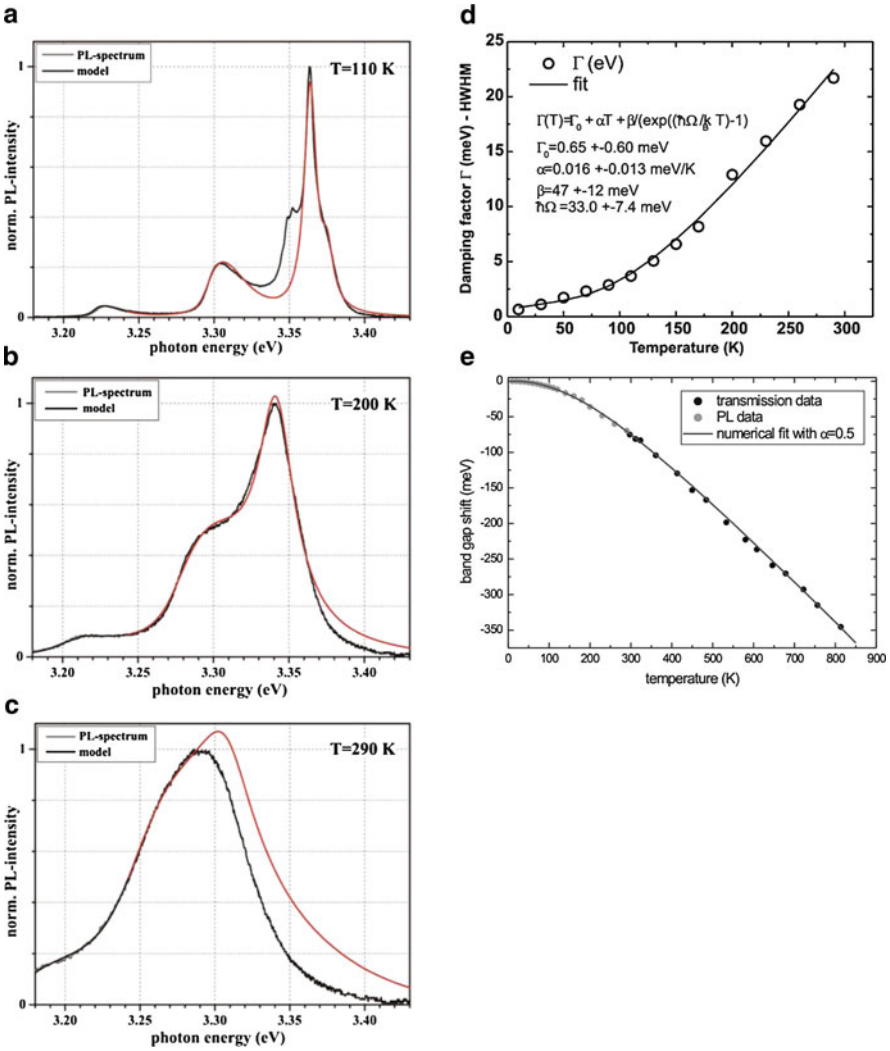

Fig. 13.13 The near edge luminescence of ZnO excited $c\omega$ in the band-to-band transition region for various temperatures with model calculations (**a**–**c**), the damping Γ of the A and B $n_B = 1\Gamma_5$ excitons as a function of temperature together with a fit function and $\sim$ parameters (**d**) and the temperature dependence of the gap with a fit function (**e**) (According to [06H1, 07K1, 07K2, 10K1, 10K2])

The temperature dependence of the band gap of ZnO deduced from luminescence and absorption data is finally given in Fig. 13.13e. The fit follows the models described in [99P1]. As a rule of thumb one can state that the gap decreases from 0 to 300 K by (90 ± 10) meV. From (13.15), and (13.16) one can deduce that the

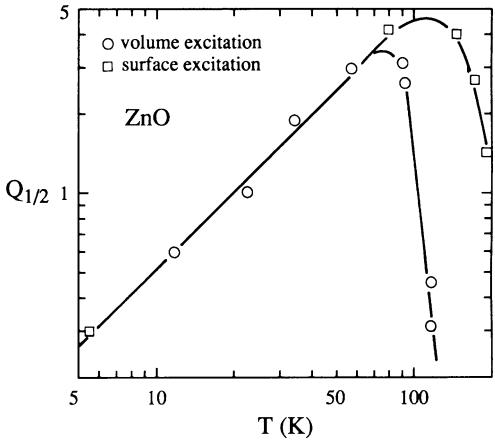

Fig. 13.14 The ratio of the integrated intensities of first and second LO-phonon replica in ZnO as a function of temperature for two different excitation conditions (According to [75K1])

ratio of the integrated intensities of the first and the second LO-phonon replica is proportional to T

$$Q_{1,2} = \frac{\int I_1^{\text{lum}}(\omega)\,\mathrm{d}\omega}{\int I_2^{\text{lum}}(\omega)\,\mathrm{d}\omega} \propto T\,. \tag{13.17}$$

In Fig. 13.14 we give experimental data for $Q_{1,2}$ in ZnO for volume excitation and surface excitation. The first case has been realized by two-photon excitation with a ruby laser, which allows relatively homogeneous excitation of samples up to thicknesses in the mm range, and the second by UV excitation in the continuum states where the excitation depth is limited mainly by diffusion to values of the order of μm as discussed above.

Up to temperatures of 100 K the points follow nicely the predictions of (13.17), then they drop. This deviation is due to reabsorption effects caused by the absorption tail described by (13.12), which starts to influence the escape depth of the polaritons also in the $m = 1$ range at higher temperatures. This effect is evidently more pronounced for volume excitation than for surface excitation. In semiconductors with less polar coupling, such as GaAs, the LO-phonon replicas are less pronounced.

For those who work on luminescent ions in insulators and are therefore familiar with the concept of the Huang–Rhys factor S, it should be mentioned that for free excitons in most semiconductors S is below one even for ones with strong ionic binding. The large ratio of first to zero phonon intensity frequently observed is not connected with a large value of S but with other processes that reduce the zero phonon emission, as outlined above (See e.g. [68V1, 79P1]). In [03Z1] the Huang-Rhys factor has been deduced from the fit of the first and second LO phonon replica in ZnSe even as a function of the kinetic energy of the exciton-like polaritons. It decreases from values around 0.3 for small $\boldsymbol{k}$ vectors to 0.1 for a kinetic energy of about 20 meV.

LO-phonon replicas do not only appear in the excitonic luminescence spectra on the low energy side, but may also appear in case of sufficiently strong exciton LO-phonon coupling in the absorption spectra on the high energy side, extending into the continuum. Examples have been cited above in connection with the term exciton-phonon bound state [66R1, 68T1, 72B1, 72K1, 94W1].

It is obvious from Figs. 13.11 or 13.13 and from the way in which the line shape of the X-mLO replica has to be fitted that a deconvolution into Gaussians is inadequate. A homogeneously broadened luminescence band has usually a Lorentian line shape, an inhomogeneously broadened one may have incidentally a Gaussian one, but there are no reasons that it has to be Gaussian, and a comparable influence of homogeneous and inhomogeneous broadening may lead to a Voigt profile. Nevertheless, one finds frequently a deconvolution of luminescence bands or even of nonlinear response functions (see e.g. references cited in [07K1, 10K1, 10K2]) into Gaussians. The reason is possibly the easy availability of the corresponding subroutine, but not arguments of physics.

The interaction of excitons and photons with acoustic phonons in Cu_2O leads to the introduction of the concept of phonoritons [00H1].

It should be mentioned that excitons can also be scattered also by emission of quasiparticles other than phonons onto the photon-like part of the polariton branch. Examples can be found, e.g., in Sect. 20.2 and we mention here scattering by magnons, which may occur in (anti) ferromagnetic semiconductors like $RbMnF_3$ or Cr_2O_3 [76S2, 99D1].

To conclude this discussion of free exciton luminescence, it should be mentioned, that a recent calculation [98K1] predicts, that a luminescence feature may occur at the position of the free exciton resonance, resulting, however, from the recombination of an electron–hole plasma (see Chap. 21) going under emission of a photon from a state containing n electron–hole pairs to one with $(n - 1)$ pairs. Though these calculations do by no means rule out the existence of excitons as good quasi-particles, a luminescence feature at the exciton energy alone is not necessarily a proof of their existence. The observation of additional features, like intra excitonic transitions (see Sect. 13.3 and [03K1, 06K1]) can help to clarify possible discrepancies. In these two references many semiconductors with small exciton binding energy have been investigated like GaAs, which show with increasing density and/or temperature readily ionization and transition to an electron-hole plasma. See Chaps. 19 and 21. In materials with larger exciton binding energy like the Cu-halides, the wide gap II–VI semiconductors, the group III nitrides or Cu_2O excitons will better survive as individual quasi-particles, though also here ionization occurs at sufficiently high densities and/or temperatures. See [07K1, 07K2, 10K1] and references therein.

As a rule of thumb it can be stated that the formation of excitons is likely for resonant and low or intermediate exciton densities (see Chap. 19 and 20). If the thermal energy $k_{\mathbf{B}}T$ is comparable to or larger than the exciton binding energy $E_{\mathrm{x}}^{\mathrm{b}}$ the excitons will be rapidly thermally ionized and have a large homogeneous width. See Fig. 13.13e. Under band-to-band excitation, exciton formation is likely for $k_{\mathrm{b}}T \ll E_{\mathrm{x}}^{\mathbf{b}}$ and for exciton formation times shorter than the electron – hole

pain lifetime. The formation time is short, if the exess energy can be dissipated by LO-phonon emission especially in polar materials, while acoustic phonon emission is slower, especially in less polar materials. We come back to this topic in Chaps. 15 and 23.

13.1.4 Spectroscopy in Momentum Space

It is clear from the above discussion that the concept of exciton polaritons allows one to understand the spectra of reflection, transmission, and luminescence, but that a quantitative interpretation of the data usually involves a rather elaborate theoretical fit. Therefore various techniques have been developed which allow more or less directly the spectroscopy of exciton polaritons in momentum space, i.e., they provide the possibility of measuring the dispersion relation $E(\boldsymbol{k})$ more directly.

In this section we therefore recall briefly the consequences of "spatial dispersion", i.e., of the dependence of ω_0 on $\boldsymbol{k}$, and then present various methods of $\boldsymbol{k}$- or momentum-space spectroscopy.

As mentioned earlier in Chap. 5, the combination of the dielectric function $\varepsilon(\omega, \boldsymbol{k})$ (6.1) and the polariton equation forms an implicit representation of the polariton dispersion. For $\omega > \omega_{0,\mathrm{L}}$ we get two propagating modes in the sample or even more if the dispersion relation is complex (Figs. 13.4b or 13.11) or if the longitudinal branch couples to the radiation field as may occur for $\boldsymbol{k} \neq 0$ or for oblique incidence in uniaxial crystals. Since the $\boldsymbol{k}$ vectors of the various modes in the sample are different, the diffracted beams propagate in different directions, thus giving some meaning to the term "spatial dispersion". Below $\omega_{0,\mathrm{L}}$ we have at least one propagating and one evanescent mode, which however, for finite damping also acquires a small real part. The consequences of this fact for the reflection spectra have already been discussed above.

The first method of $\boldsymbol{k}$-space spectroscopy uses the analysis of the Fabry–Perot modes introduced in Sect. 3.1.6, which appear for example in as-grown, thin, platelet type samples with plane-parallel surface. For an example see Fig. 13.9b. As already pointed out there, transmission maxima occur when an integer number of half-waves fit into the resonator, i.e.,

$$k_m(\omega_m) = m\frac{\pi}{d}\,,\ m = 1, 2, 3\ldots\,, \tag{13.18}$$

where d is the geometrical thickness of the sample and k is the real part of the wave vector in the medium. If ω_m and k_m are known for one m_1 then the dispersion relation can be reconstructed from (13.18) by reading the $\hbar\omega_m$ from the transmission spectrum and by progressing in steps of πd^{-1} on the k-axis. In Fig. 13.15 we show the dispersion of the $n_{\mathrm{B}} = 1$ A-Γ_5-exciton polariton in CdSe, together with a measured and a calculated reflection spectrum. The condition for the reflection minima coincides with that for the transmission maxima in (13.18).